

# Coastline changes detection from Sentinel–1 satellite imagery using spatial fuzzy clustering and interactive thresholding method in Phan Thiet, Binh Thuan

Nhi Huynh Yen <sup>1\*</sup>, Thoa Le Thi Kim<sup>1</sup>

<sup>1</sup> Ho Chi Minh City University of Natural Resources and Environment;  
nhih@hcmunre.edu.vn; thoa.ltk@hcmunre.edu.vn

\* Correspondence: nhih@hcmunre.edu.vn; Tel.: +84906263355

Received: 12 August 2020; Accepted: 12 October 2020; Published: 25 December 2020

**Abstract:** The coastline is an important component of coastal management studies. The coastline changes rapidly over time, therefore it is necessary to have methods of monitoring the shoreline quickly and continuously. In this study, Sentinel–1A satellite imagery is used to extract the coastline in Phan Thiet City. The boundary between land and water is determined by a two–step process: fuzzy clustering and interactive thresholding. Subsequently, the coastline in the study area was extracted into vector form. Finally, this shoreline is compared to manually digitized shoreline. There are 350 locations considered to determine the distance between two shorelines, of which 274 locations (77%) are 0 to 5 m (equivalent to ½ pixel) and 76 (23%) locations are over 5 m. In addition, the DSAS statistics has also provided a detailed view of the seasonal change of shoreline for two years (2016 and 2017). The study results showed that effective application capabilities of Sentinel–1A radar satellite image data to quickly assess the erosion/accretion of coastal areas.

**Keywords:** Shoreline extraction; Sentinel–1A; Fuzzy clustering; Interactive thresholding.

---

## 1. Introduction

The shoreline is considered as one of the most dynamic linear features in the coastal [1] and it is simply defined as the physical interface between land and water [2]. The location of the shoreline changes continually through time under the influence of ocean elements (tides, waves, wind), coastal geomorphology contexts (erosion, accretion) as well as the human social and economic activities [3]. Therefore, researchers have used the term instantaneous shoreline to describe the position of the land–water interface in a certain time [4–5]. Determining shoreline change through time are required for application to in direction of sediment transport [6–8], monitoring coastal erosion/accretion [9–11] and management of coastal resources [12].

The shoreline position changes were obtained by collecting data and extracting shoreline information from ground surveying and aerial photography, but it is expensive and time–consuming methods [13–15]. Alternatively, the shorelines can be extracted directly through the analysis of satellite imagery data [16], including the use of multispectral/hyperspectral satellite images [17–21] and radar images [22–24]. The satellite image is being widely used in the detection of the coastline changes by setting a threshold for land and water separations which proved a cost–effective approach for the study of the coast. Based on the spectral reflectance of land and water, the optical images provide a simple way to extract shorelines. Unfortunately, those images are sensitive to weather conditions, especially in tropical marine climate areas. Radar interacts with the surface features in ways different from the optical radiation. Radar images receive the contrast of the dielectric properties and surface roughness

to determine the boundary between land versus water [25–26]. Besides, the microwave energy radar is capable of penetrating cloud cover and sensing at night, so it is suitable for shoreline positions changes monitoring at short (monthly) intervals. In recent years, the shoreline indicators corresponding with reference to different tidal datums can be derived easily by light detection and range (LiDAR) data which are acquired at a low water level [27–28]. However, the created shoreline is often broken [29–30] and LiDAR is an expensive technique [31], therefore it is not suitable for continuous coastal monitoring with limited funding. In this research, the Sentinel-1 SAR (Synthetic Aperture Radar) satellite imagery data provided by European Space Agency (ESA) is used to extract shoreline information.

The interpretation of SAR images is difficult because of the presence of speckle noise and non-uniform signal characteristics [32]. In recent years, there are many studies involving the improvement of methods for extraction of coastlines from SAR data, such as edge detection and edge-tracing algorithm [33–35] setting threshold [36–38]; active contour model [39] clustering [40–43] or combining methods [43–45]. In particular, the clustering method is considered to be the removal of speckle noise from the satellite images [46].

Erteza extracted the shoreline automatically from SAR images based on the development of 3 algorithms [36]. Including, histogram equalization is used to accentuate the land/water boundary on pre-processing steps. The next step, a threshold is set to maximum filter to enhance the land–water boundary and produces a single-pixel-wide coastline. Finally, the contour tracing algorithm is applied to mark a single pixel wide as small islands. Modava presented an efficient approach to extracting coastlines from high-resolution SAR images [43]. The first, spatial fuzzy c-means clustering is applied to cluster pixel values into two classes of land and water. After that, reasonable threshold used to segment on the fuzzification results using Otsu's method and morphological filters are used to eliminate spurious segments on the binary image. Third, the active contour level set method was applied to refine the segmentation. Demir et al. proposed a fuzzy logic approach to classify the land and water pixels [47–48]. Pre-processing of SAR image is consisting of reducing radar noise and speckle by Lee filter using and terrain correction by the Shuttle Radar Topography Mission (SRTM) digital surface model. Then, the fuzzy clustering using mean standard deviation method is applied to classify the preprocessing result with calculated parameters. In the post-processing step, the morphological filter is applied to remove the zigzag effects of the detected shorelines.

In this present study, fuzzy membership functions are applied to assign fuzzy membership values to crisp values which has been successfully applied in the SAR image analysis by Demir et al [47–48]. The next method used in the shoreline extraction process is the application of an appropriate threshold for segmenting the image. From the result of determining the boundary between land and water, the data is converted to vector. The Digital Shoreline Analysis System (DSAS) used to calculate differences in the shoreline rates, which are extracted from the fuzzy clustering–interactive thresholding method and manually digitized method. Finally, a short analysis is used to compare the differences in the shoreline between two seasons of the year.

## 2. Materials and Methods

### 2.1. Study Area

A portion of Binh Thuan Province coast was selected as the study area, which its length is approximately 90 kilometers. Located in the Southeast Region of Vietnam, its geographical coordinate has the range of the longitude (105°48'33"E–107°35'58"E) and latitude (10°19'13"N–12°17'54") in Figure 1.

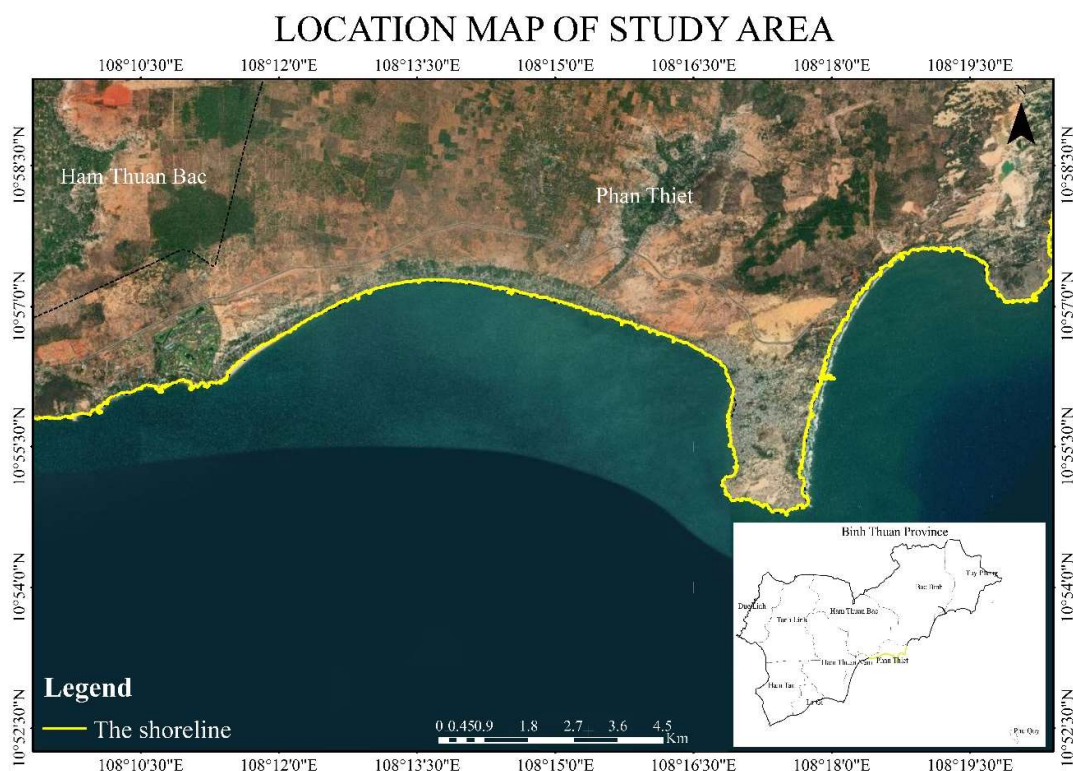


**Figure 1.** Map of the study area.

The study area province is located in the tropical monsoon region, with two main wind directions: Northeast (from November to April) and Southwest (from May to October). The average yearly temperature is 27 °C and average rainfall is 1,024 mm. The average tide range is 2–3 meters [49]. This coastal area has enormous potential for aquaculture, seaports and especially for tourism. However, the coast has been experiencing severe erosion for years, although eroded sections have been constructed for protection. Some studies have shown that the construction of breakwaters affects the erosion–accretion law in this area. Understand the causes and rules of erosion–accretion is necessary to support the development of effective technical solutions for the planning and sustainable development of Binh Thuan's coastal zone.

## 2.2. Data Sets

To extract the shoreline from SAR data, Sentinel–1 images are obtained free of charge from European Space Agency (ESA) Sentinels Scientific Data Hub. The Sentinel–1 is the radar imaging mission, which provides continuous all–weather day/night imagery for land and ocean services at C–band with a repeat cycle of 12 days (a single satellite) or 6 days (two–satellite constellation). The dataset in this research for the extraction of the shoreline is two images of Sentinel–1 IW Level 1 GRD data acquired in VH/VV polarization with the ground resolution 10m.

For SAR image time series analysis, the time to collect image data sentinel should depend on the following factors: representing the northeast and southwest wind seasons, suitability of tide data and image acquisition. First, to describe the change of coastline in two seasons with different wind direction and wave direction, satellite imagery data will be collected in June–July and November–December. Secondly, attention should be paid to the

characteristics of the tide because the shoreline is a dynamic line ranging between high and low tide.

A number of studies have adjusted tide-coordinated shoreline-based tide data, field data, digital model... However, this correction process is often difficult and inaccurate. In this study, based on the collected tide data at the Vung Tau tide gauge, both SAR images were acquired at equal high tide conditions (3,2 m), which are described in Table 1.

**Table 1.** Characteristics of Sentinel-1A level 1 GRD IW product used in this study.

Image		Max Tide	
Date	Acq. GMT (HHMM)	Acq. GMT (HHMM)	H (m)
Aug 2016	22:36	23:00	3.2
01 Dec 2016	22:36	23:00	3.2
06 Jul 2017	11:02	11:00	3.2
15 Nov 2017	11:03	11:29	3.2

### 2.3 Methodology

The implementation method consists of five steps as shown in Figure 2.

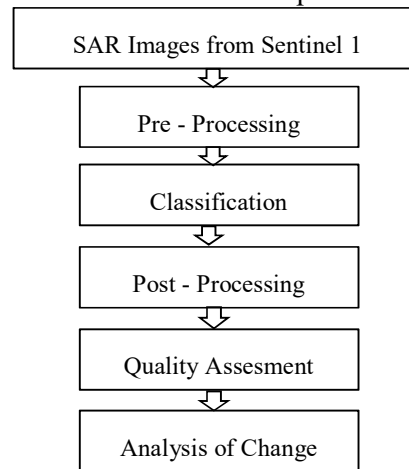


**Figure 2.** Processing workflow.

#### 2.3.1 Pre-Processing SAR Images

All the obtained Sentinel images are refined with the orbit files which provides accurate satellite position and velocity information of each product. The data is acquired from the same sensor at different times, so radiometric correction is necessary for converting digital pixel values to radar backscatter in SAR images. The Lee filter, one of the spatial filtering methods is applied to reduce speckle noise and non-uniform signal characteristics of the signals returning from the ocean surface for calibrated SAR images. Then, filtered images are terrain-corrected using SRTM digital surface model for the purpose of repairing geometric distortions that lead to geolocation errors. The geographic coordinate system is the World Geodetic System 84 (WGS 84) and the selected projection is UTM zone 49 North. The SAR data are preprocessed by the open source software SNAP Toolbox which is provided by the European Space Agency (Figure 3).

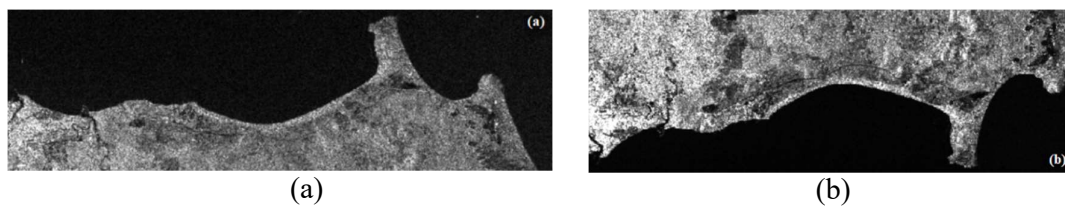


**Figure 3.** (a) Original SAR image; (b) image after Pre-Processing.

### 2.3.2 Determining of Land and Sea

The boundary between land and water is determined through a two-step process: fuzzy clustering and interactive thresholding. The ArcGIS software is used for solving the problem of determining of land and sea. Firstly, the fuzzy membership functions are used to transform the averaged SAR image to a 0 to 1 possibility scale based on the designation of membership to a specified set. Because the average and standard deviations between soil and water pixels are very large, the fuzzy clustering function is set according to the formula (1) to optimize the data dispersion:

$$\mu(x) = 1 - \frac{bs}{x-am+} \quad \text{if } x > am \quad \text{otherwise } \mu(x) = 0 \quad (1)$$

where  $m$  is the mean;  $s$  is the standard deviation;  $b$  and  $a$  are multipliers.

To initialize fuzzy membership function, a series of empirical values used for selection of the multipliers  $a$  and  $b$ . Experimental results show that  $a = 0.43$  and  $b = 0.04$  are appropriate to maximize the land surface membership of the study area. The results of using fuzzy clustering are shown in Figure 4.

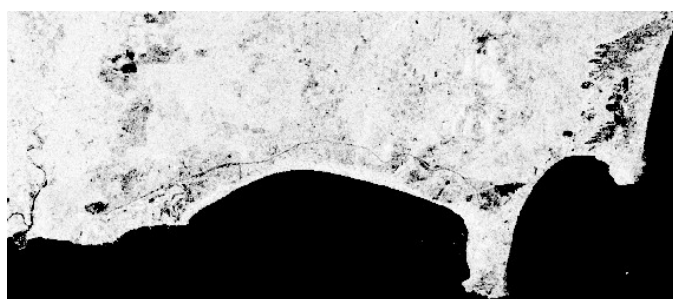


**Figure 4.** Results of applying fuzzy clustering.

At the next result of methodology, an optimal histogram thresholding in this case is 0.502, which is used to create binary images. The boundary between land and water is defined as a sign for extracting the shoreline. The created binary image contains pixel values of 1 (Red) or 0 (black), where the pixel values above the defined threshold was divided into the land (Red) and the opposite was divided into the sea (black). The boundary between the land and the water on the binary image is determined to extract the shoreline (Figure 5).



**Figure 5.** Result of applying the threshold for separation between land (red) and water (black).

### 2.3.3 Extraction of the shoreline data

After separation between the land and sea, the segment results are further processed as extraction of the line from the region–segmented result, generalizing to eliminate the lines zigzag vectors (Figure 6).

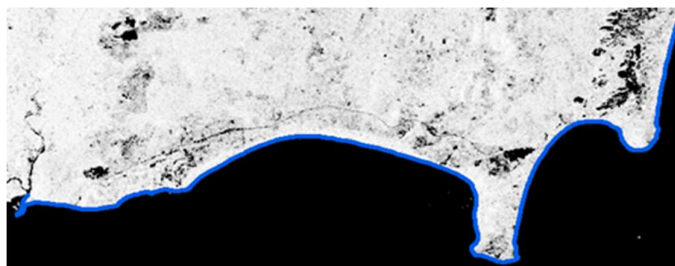


**Figure 6.** The shoreline results were extracted from the Sentinel–1A satellite image.

## 3. Results and Discussion

The shoreline result (15 Nov 2017) is assessed with digitized manual shoreline, by calculating the perpendicular distance between the two shorelines. The extracted shoreline from the digitization method are shown in Figure 7.

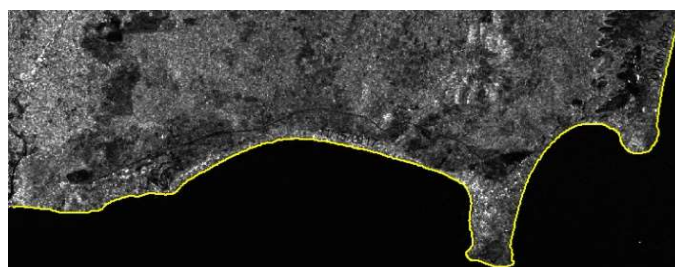


**Figure 7.** The shoreline results were extracted from the Sentinel–1A satellite image using digitization.

The DSAS (Computer Software for Calculating Shoreline Change) tool is used to calculate differences in the shoreline rates, which are extracted from the fuzzy clustering – interactive thresholding method and manually digitized method (Figure 8).

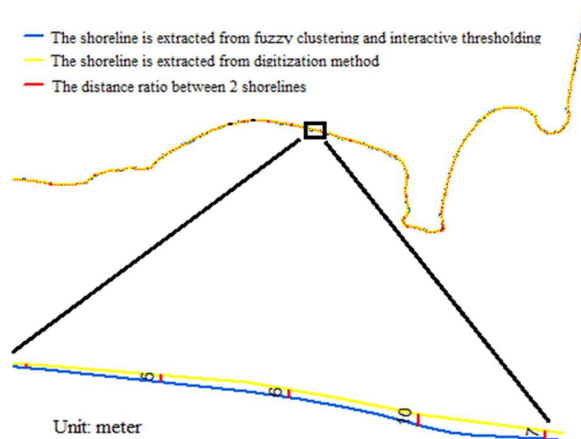


**Figure 8.** The location of the distance lines between the two shorelines is determined by the DSAS tool (15 Nov 2017).

Statistical results for 350 locations to calculate the distance between the two shoreline results are shown in Figure 9.

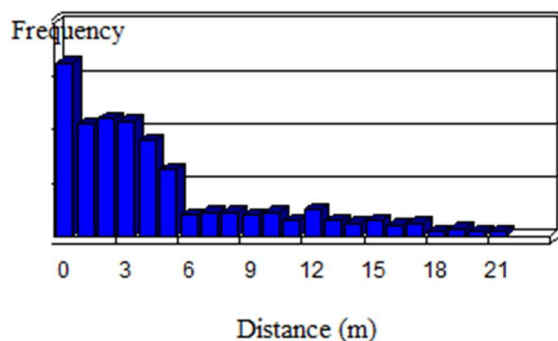


**Figure 9.** Differences in distance between 2 shorelines.

Of which, 274 (77%) locations had a distance between the 2 shorelines from 0 to 5 m (equivalent to the error of half a pixel), 76 (23%) of positions had a distance between the two shorelines over 5 m. The average distance between two coastlines is 3 m, the longest distance is 13 m. The results show that it is possible to clearly distinguish the boundary between land and water through the extraction of the shoreline from the Sentinel-1A satellite image fuzzy clustering and interactive thresholding. Further, additional field survey data or other data sources are needed to assess the accuracy of the result.

To consider how the wind factor affects the shoreline morphology, the DSAS tool is also used to analyze the position change of the shoreline over two seasons of the year. The Mui Ne and Hon Rom areas represent the study area. The results of extracting the shoreline from Sentinel-1 SAR images at 4 periods are shown in Figure 10.

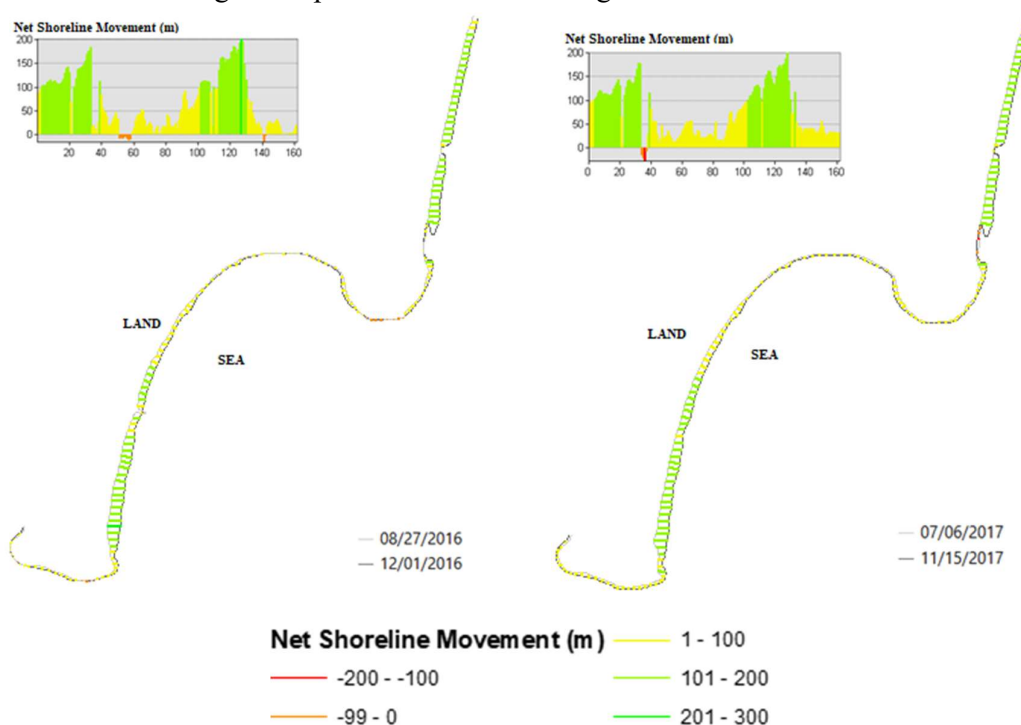


**Figure 10.** The shoreline results were extracted from the Sentinel-1A satellite image using digitization at 4 periods.

The DSAS statistics provided a detailed view of the seasonal change of shoreline for two years on the Binh Thuan coast. The results show similarity in the morphological change of the shoreline. During the southwest monsoon (from May to October), the coastline in the wind-receiving area tends to move inland. On the contrary, during the southeast monsoon (from November to April), the coastline tends to shift to the sea. The above results will be used for other research purposes in the future.

#### 4. Conclusion

The results of the extracted shoreline from the Sentinel-1A satellite image show the applicability of radar satellite imagery in coastal monitoring. Sentinel-1A satellite image is not affected by weather, can be monitored over a large area, high spatial resolution and provided free of charge. These are important data sources and they can satisfy the need for continuous coastal monitoring. From there, it helps to support the right plans for erosion and deposition in the coastal area.

**Author Contributions:** Conceptualization, Thoa, L.T.K.; Data sets, Nhi, H.Y.; Methodology, Nhi, H.Y.; Software, Nhi, H.Y.; Verification of results, Thoa, L.T.K.; Writing—original draft preparation, Nhi, H.Y.; Writing—review and editing, Thoa, L.T.K., Nhi, H.Y.

**Conflicts of Interest:** The authors declare no conflict of interest.

#### References

1. Winarso, G.; Budhiman, S. The potential application of remote sensing data for coastal study. Proceedings of the Asian Conference on Remote Sensing, Singapore. 2001.
2. Dolan, R.; Hayden, B.P.; May, P.; May, S. The reliability of shoreline change measurements from aerial photographs. *Shore Beach* **1980**, *48*, 22–29.
3. Boak, E.H.; Turner, I.L. Shoreline definition and detection: a review. *J. Coastal Res.* **2005**, 688–703.
4. Morton, R.A. Accurate shoreline mapping: past, present, and future. Proceedings of the Coastal Sediments, ASCE, 1991.
5. Smith, G.L.; Zarillo, G.A. Calculating long-term shoreline recession rates using aerial photographic and beach profiling techniques. *J. Coastal Res.* **1990**, 111–120.
6. Eriksson, E.L.; Persson, M.H. *Sediment transport and coastal evolution at Thuan An Inlet*, Vietnam, 2014.
7. Ali, T. Along-shore sediment transport estimation and shoreline change prediction: a comparative study. Whitepaper—uploadfile, Department of Engineering Technology University of Central Florida, viewed, 2009.
8. Williams, J.J.; Esteves, L.S. Predicting shoreline response to changes in longshore sediment transport for the Rio Grande do Sul coastline. *Braz. J. Aquat. Sci. Tech.* **2008**, *10*, 1–9.
9. Leatherman, S.P. *Coastal erosion: mapping and management*. Coastal Education & Research **1997**, 24.
10. Kannan, R.; Ramanamurthy, M.V.; Kanungo, A. Shoreline Change Monitoring in Nellore Coast at East Coast Andhra Pradesh District Using Remote Sensing and GIS, Proceedings of the Fisheries Livest, 2016.
11. Zhang, K.; Douglas, B.C.; Leatherman, S.P. Global warming and coastal erosion. *Clim. Change.* **2004**, *64*, 41–52.
12. Shetty, A.; Jayappa, K.S.; Mitra, D. Shoreline change analysis of Mangalore coast and morphometric analysis of Netravathi–Gurupur and Mulky–Pavanje spits. *Aquat. Procedia.* **2015**, *4*, 182–189.

13. Leatherman, S.P. Shoreline mapping: a comparison of techniques. *Shore Beach* **1983**, *51*, 28–33.
14. Li, R.; Di, K.; Ma, R. A comparative study of shoreline mapping techniques. *GIS Coastal Zone Manage.* **2001**, 53–60.
15. Dolan, R.; Fenster, M.S.; Holme, S.J. Temporal analysis of shoreline recession and accretion. *J. Coastal Res.* **1991**, 723–744.
16. Gens, R. Remote sensing of coastlines: detection, extraction and monitoring. *Int. J. Remote Sens.* **2010**, *31*, 1819–1836.
17. Chen, L.C.; Shyu, C.C. Automated extraction of shorelines from optical and SAR images. Proceedings of the Asian Conference on Remote Sensing, Manila, Philippine, 1998.
18. Ouma, Y.O.; Tateishi, R. A water index for rapid mapping of shoreline changes of five East African Rift Valley lakes: an empirical analysis using Landsat TM and ETM+ data. *Int. J. Remote Sens.* **2006**, *27*, 3153–3181.
19. Sekovski, I.; Stecchi, F.; Mancini, F.; Rio, L.D. Image classification methods applied to shoreline extraction on very high-resolution multispectral imagery. *Int. J. Remote Sens.* **2014**, *35*, 3556–3578.
20. Behling, R.; Milewski, R.; Chabrilat, S. Spatiotemporal shoreline dynamics of Namibian coastal lagoons derived by a dense remote sensing time series approach. *Int. J. Appl. Earth Obs. Geoinf.* **2018**, *68*, 262–271.
21. Zulkifle, A.A.; Hassan, R.; Othman, R.M.; Sallow, A.B. Supervised classification and improved filtering method for shoreline detection. *J. Theor. Appl. Inf. Technol.* **2017**, *95*, 5628–5636.
22. Lee, J.S.; Jurkevich, I. Coastline detection and tracing in SAR images. *IEEE Trans. Geosci. Remote Sens.* **1990**, *28*, 662–668.
23. Braga, F.; Tosi, L.; Prati, C.; Alberotanza, L. Shoreline detection: capability of COSMO–SkyMed and high-resolution multispectral images. *Eur. J. Remote Sens.* **2013**, *46*, 837–853.
24. Heine, I.E. Long-term monitoring of lakes in the northern central European lowlands using optical and radar remote sensing imagery. Doktor der Naturwissenschaften, Berlin, 2017.
25. Rozenstein, O.; Siegal, Z.; Blumberg, D.G.; Adamowski, J. Investigating the backscatter contrast anomaly in synthetic aperture radar (SAR) imagery of the dunes along the Israel–Egypt border. *Int. J. Appl. Earth Obs. Geoinf.* **2016**, *46*, 13–21.
26. MacDonald, H.C.; Lewis, A.J.; Wing, R.S. Mapping and Land form Analysis of Coastal Regions with Radar. *Geol. Soc. Am. Bull.* **1971**, *82*, 345–358.
27. Yousef, A.; Iftekharruddin, K. Shoreline extraction from the fusion of LiDAR DEM data and aerial images using mutual information and genetic algorithms. In Neural Networks (IJCNN), Proceedings of the International Joint Conference, 2014.
28. Liu, H. Shoreline mapping and coastal change studies using remote sensing imagery and LIDAR data. Proceedings of the Remote sensing and geospatial technologies for coastal ecosystem assessment and management, 2009.
29. Caixia, Y.; Jiayao, W.; Jun, X. Advance of coastline extraction technology. *Int. J. Geomatics Geosci.* **2014**, *31*, 305–309.
30. Stephen P Leatherman, Shoreline change mapping and management along the US East Coast. *J. Coastal Res.* **2003**, 5–13.
31. Vandebroek, E.; Lindenbergh, R.; van Leijen, F.; de Schipper, M.; de Vries, S.; Hanssen, R. Semi-Automated Monitoring of a Mega-Scale Beach Nourishment Using High-Resolution TerraSAR-X Satellite Data. *Remote Sens.* **2017**, *9*, 653.
32. Goodman, J.W. Some fundamental properties of speckle. *JOSA* **1976**, *66*, 1145–1150.
33. Liu, H.; Jezek, K.C. Automated extraction of coastline from satellite imagery by integrating Canny edge detection and locally adaptive thresholding methods. *Int. J. Remote Sens.* **2004**, *25*, 937–958.

34. Buono, A.; Nunziata, F.; Mascolo, L.; Migliaccio, M. A multipolarization analysis of coastline extraction using X-band COSMO–SkyMed SAR data. *IEEE J. Sel. Top. Appl. Earth Obs. Remote Sens.* **2014**, *7*, 2811–2820.
35. Sheng, G.; Yang, W.; Deng, X.; He, C.; Cao, Y.; Sun, H. Coastline detection in synthetic aperture radar (SAR) images by integrating watershed transformation and controllable gradient vector flow (GVF) snake model. *IEEE J. Oceanic Eng.* **2012**, *37*, 375–383.
36. Erteza, I.A. *An automatic coastline detector for use with SAR images*. Sandia National Laboratories (SNL–NM), Albuquerque, NM, 1998.
37. Markiewicz, L.; Mazurek, P.; Chybicki, A. Coastline change–detection method using remote sensing satellite observation data. *Hydroacoustics*. **2016**, *19*, 277–284.
38. Bioresita, F.; Hayati, N. Coastline changes detection using Sentinel–1 satellite imagery in Surabaya, East Java, Indonesia. *Geoid*. **2016**, *11*, 190–198.
39. Zhang, H.; Zhang, B.; Guo, H.; Lu, J.; He, H. An automatic coastline extraction method based on active contour model. Proceedings of the Geoinformatics (GEOINFORMATICS) International Conference, 2013.
40. Baselice, F.; Ferraioli, G. Unsupervised coastal line extraction from SAR images. *IEEE Geosci. Remote Sens. Lett.* **2013**, *10*, 1350–1354.
41. Liu, Y. Coastline detection from remote sensing image based on K–mean cluster and distance transform algorithm. *Adv. Mater. Res.* **2013**, 760–762, 1567–1571.
42. Ning, J.; Zhang, L.; Zhang, D.; Wu, C. Interactive image segmentation by maximal similarity based region merging. *Pattern Recognit.* **2010**, *43*, 445–456.
43. Modava, M.; Akbarizadeh, G. A level set based method for coastline detection of SAR images. Proceedings of the Pattern Recognition and Image Analysis International Conference, 2017.
44. Paes, R.L.; Nunziata, F.; Migliaccio, M. Coastline extraction and coastal area classification via SAR hybrid–polarimetry architecture. Proceedings of the Geoscience and Remote Sensing Symposium (IGARSS), 2015.
45. Liu, Z.; Li, F.; Li, N.; Wang, R.; Zhang, H. A novel region–merging approach for coastline extraction from Sentinel–1A IW mode SAR imagery. *IEEE Geosci. Remote Sens. Lett.* **2016**, *13*, 324–328.
46. Modava, M.; Akbarizadeh, G. Coastline extraction from SAR images using spatial fuzzy clustering and the active contour method. *Int. J. Remote Sens.* **2017**, *38*, 355–370.
47. Demir, N.; Kaynarcaa, M.; Oya, S. Extraction of coastlines with fuzzy approach using SENTINEL–1 SAR image. ISPRS–International Archives of the Photogrammetry, Proceedings of the Remote Sensing and Spatial Information Sciences, 2016.
48. Demir, N.; Oy, S.; Erdem, F.; Şeker, D.Z.; Bayram, B. Integrated shoreline extraction approach with use of Rasat MS and Sentinel–1a SAR images. ISPRS Annals of Photogrammetry, Proceedings of the Remote Sensing & Spatial Information Sciences, 2017.
49. Long, B.H. Một số kết quả khảo sát, nghiên cứu hiện tượng xói lở, bồi tụ khu vực ven biển Bình Thuận, 2004.